Joint dissolution and oxidation behaviour of 316LN steel at 550°C in liquid sodium containing low concentration of oxygen

J. L. Courouau, Matthieu Rivollier, V. Lorentz, Michel Tabarant

Proceedings of ICAPP 2015
May 03-06, 2015 - Nice (France)
Paper 15417

Joint dissolution and oxidation behaviour of 316LN steel at 550°C in liquid sodium containing low concentration of oxygen

Jean-Louis Courouau[1]; Matthieu Rivollier[1]; V. Lorentz[1], Michel Tabarant[2]
[1]CEA, DEN, DANS, DPC, SCCME, Laboratoire d'Etude de la Corrosion Non Aqueuse, F-91191 Gif-sur-Yvette, France
[2]CEA, DEN, DANS, DPC, SEARS, Laboratoire d'Ingénierie des Surfaces et Lasers, F-91191 Gif-sur-Yvette, France
Tel: +33169081643, Fax: +33169081586, Email: jean-louis.courouau@cea.fr

Abstract – *The sodium cooled fast reactor is selected in France as the 4th generation of nuclear power plant. 4th generation's reactor vessel, primary loop structures and heat exchangers will be made of austenitic stainless steels (316LN). To assess reactor service life time, corrosion of austenitic stainless steel by liquid sodium is studied in normal operating conditions as well as in transient conditions either expected or not. Oxygen, one of the main impurities, but present in trace amounts (1 to 10 µg/g or ppm weight), plays a major role on corrosion phenomena of the steel, although not totally understood yet. Literature reports an increased dissolution rate of steel or even of pure iron with increasing oxygen content although no thermodynamically stable iron oxide exists at low oxygen content. Oxygen is only known to form sodium chromite scale ($NaCrO_2$), those behaviour is, however, little documented. Based on corrosion tests performed in the static sodium test device ("CorroNa") at 550°C for an oxygen content initially of about 1 ppm in weight or lower, and about 5-10 ppm after 4600h of test, either a really small dissolution rate or small sodium chromite scale formation ($NaCrO_2$) are observed. Dissolution and carburation are observed for specimen immersed since the beginning of the test, while oxidation is the main feature observed for the specimen immersed during the last periods of the test. Some aspects of the morphologies of this oxide scale obtained by scanning electron microscopy (SEM) or transmission electron microscopy (TEM) as well as by Glow Discharge Optical Emission Spectroscopy (GD-OES) are presented. Discussions and explanations of these apparently opposing results are given based on thermodynamic analysis, as well as their possible consequences for reactor operation.*

I. INTRODUCTION

The use of liquid sodium at high temperature on the long term is envisaged as coolant for Sodium Fast Reactors (SFR), which are being evaluated by CEA for a future generation of nuclear reactors (60 years – 350°C to 550°C) [1]. The chemical conditions of impurities present in trace levels in the liquid sodium may vary with the operating time (normal, transient and incidental), meaning that any interactions of the liquid metal with structural materials must be well known, well understood, and possibly predicted to guarantee service life-time as well as resistance to incidental conditions, even though the corrosion related phenomena of austenitic steels are reported as limited both by literature and by operational feedback from built reactors [2, 3]. However, longer service-life time and chemical transients are now reconsidered [4-7]. One of the main corrosion parameters apart from the temperature and the hydrodynamics of the liquid metal is the dissolved oxygen content, as it stands for one of the most important impurity in such liquid metal systems. Although its exact role is still unknown, oxygen is reported to increase the corrosion even at the traces levels either by catalysing the dissolution of iron (but not of nickel) or by promoting excessive mass transfer [8-10].

The dissolution phenomena is described as an homogeneous dissolution of the alloying element of the steels, which steady state is achieved after a transient driven by reduction of native oxides and preferential leaching of some elements (Ni, Cr, Mn, C) that lead to the transformation of surface layer of the austenite into ferrite scale after a few hundreds to a few thousands of hours depending of the temperature. This scale then controls the homogeneous dissolution of the steels by acting as a diffusion barrier. Dissolution is reported to become significant above 600°C and lies in the range of ~1-10 µm of steel dissolved per year in addition to the 1-10 µm of degraded austenite. Semi–empirical corrosion models are available [11, 12], which can be used to assess the mass transfer of activated corrosion products such as ^{60}Co or ^{54}Mn in the primary systems [10]. Extrapolation on the long term, however, fails to predict the extent of the corrosion observed of sample presenting 10^5h of operation [13]. For slightly higher oxygen content (few ppm), oxygen forms a ternary oxide scale of $NaCrO_2$ (sodium chromite) on chromium alloyed steels interface in specific conditions [14] and accelerates intergranular penetration for higher oxygen levels [15, 16]. Qualitatively, 2 separate corrosion domains may be defined: oxidation by the formation of sodium chromite scale when the oxygen

activity is high enough and dissolution of the steels when the oxygen activity is low enough. Oxygen threshold can be figured out by thermodynamic relations as function of the temperature and chromium activity of the interface where reaction takes places. Result depends of the data used such as the oxygen solubility and the free energies of formation of the double oxide. For instance, the critical oxygen content at 500°C for the sodium chromite formation is given by Shaiu [17] as 2.2 ppm for unit activity of chromium. This concentration is within the expected concentration range for reactors operations (1-10 ppm), meaning that the thermodynamics conditions for oxidation is encountered in reactor systems.

It is thought that oxidation takes a non-negligible part on the overall corrosion kinetics, as a result of successive or simultaneous corrosion mechanisms [18], inducing the need for an accurate reassessment of each mechanism's independently from each other's. This required the development of liquid metal setup for separate effect studies [6]. While the oxidation mechanism is under study elsewhere [16, 18-19], as oxidation mechanism was up to now little documented although regularly observed, the objective of the test presented here is to reinvestigate mechanisms of dissolution at 550°C in low oxygen content in order to characterise morphologies at the finest scale available by scanning and transmission electron microscopes (SEM, TEM) and surface characterization using glow discharge-optical emission spectrometry (GD-OES).

II. MATERIAL AND CORROSION CONDITIONS

The tested material is an austenitic stainless steel of the grade X2CrNiMo17-12-2, nitrogen controlled, elaborated in accordance with the RCC-MR codification (RM 3331 level 2). After rolling, the steel was annealed at 1120°C and quenched in water. Its composition is given in Table I. Mean grain size is between 30 to 40 µm. The specimens were machined by wire electrical discharge machine (EDM).

The tests are run in a static sodium device "CorroNa" [6]. The sodium is contained in a molybdenum crucible. A furnace heats the thermal well where the crucible is set. All of this is set below an argon purified glove box that simplifies all operations required for preparation of the test and handling of the liquid metal. During corrosion test, the system is perfectly tight towards both the atmosphere and the argon of the gloves box. Before testing, the 99.95 % pure sodium (provided by Métaux Spéciaux - ER grade) is melted and the free level is skimmed out in order to remove sodium oxide present in excess. A low temperature step at 108°C is done for 300 hours (decantation) followed by skimming out any residual oxides present at the free level. Then, a last purification step is done at high temperature (628°C during 75 h) with large surface zirconium foil (150x300x0.125 mm) to getter any residual oxygen. This foil is removed after the purification step. The oxygen is then assessed to 1 ppm or lower. The qualitative appearance of the free level confirmed this assessment (perfect mirror). The specimens are then immersed in liquid sodium at 110°C and the system is tightly closed. Sodium is heated to 550°C at 0.5°C/min. The temperature is kept constant for several days or weeks and decreased at 0.5°C/min, to remove one set of sample and reintroduce another specimen. 5 exposure periods were done on that same principle: 650h (1) – 900h (2) – 1500h (3) – 900h (4) and 650 hours (5), roughly, in order to double the sample exposed during the same duration, respectively 650h (period 1 or 5), 1500h (periods 1+2 or 4+5), 3050h (periods 1+2+3 or 3+4+5), 3950h (periods 1+2+3+4 or 2+3+4+5), and 4600h (periods 1+2+3+4+5, both specimens). It is critical to note that half of the specimens are exposed from the beginning of the test while others were exposed during the last periods of the test. Others specimens were exposed during the same tests, such as steels (Fe-9Cr-1Mo, 800 alloys, pure Ni, Fe, & Hf) or ceramics (Alumina, hafnie). The surface over volume ratio is estimated to 0.9 dm^{-1}, mainly due to the steels specimens (3 dm^2/2.8 dm^3 of sodium). After immersion in liquid sodium, the specimens are washed with 99.9 % pure ethanol (provided by Carlo Erba) in order to remove metallic sodium from the sample surfaces and are stored in desiccators. After the first washing and weighting, a second rapid cleaning in pure water is performed.

TABLE I
Composition of the 316LN stainless steel tested.

Element	Concentration (wt. %)
Fe	Balanced
Cr	17.27
Ni	12.13
Mo	2.54
Mn	1.74
C	0.026
Si	0.31
P	0.025
S	0.001
N	0.069
B	0.0004
Cu	0.0029
Co	0.09

The specimens are then weighted to get the weight variation. Morphological characterizations are performed by means of electron microscopy: Scanning Electron Microscopy (SEM), the device Zeiss - Gemini ultra 55 is used to characterize surface and specimen cross-sections. In both cases, Energy Dispersive X-ray analyses are done (EDX, device: Bruker AXS Flash Detector 4010). Depth elementary profiles are obtained from the interface by Glow Discharge Optical Emission Spectroscopy (GD-OES, device: Horiba Jobin Yvon GD-Profiler 2). The

concentration profiles are performed on a 4 mm diameter area, with a 2.5 nm depth resolution. In addition, a thin slice is extracted from one the 2 specimens exposed during 4600 h from the beginning of the test by using a focused ion beam (FIB) mounted in a SEM STRATA 400S (FEI) after the deposition of a tungsten layer on the surface. The slice is cut and pasted to a Mo grid. Molybdenum was preferred to copper for the grid to allow for a better detection of sodium. After an additional ions thinning step, the slice was observed by transmission electron on the Osiris device from Tecnai at 200 kV. Transmission electron microscopy (TEM), high resolution TEM (HRTEM), scanning TEM (STEM), EDX and EELS were the techniques used for imaging and analysing. The use of the molybdenum grid prevents any quantification of the Mo element by EDX.

III. RESULTS AND DISCUSSION

The 316LN specimens present 2 distinct behaviours depending of the period of exposition, either from the beginning or for the last periods of the test. These separate behaviours happen despite the fact that the specimens were exposed to liquid sodium for at least one common exposure period. While the weight variation is positive in both cases, the net weight gain is about 100 times higher for the specimen exposed for the last 650h when compared to the specimen exposed for the first 650h: 0.5 to 0.005 mg/dm²/day. Based on the weight variation of all specimens, the kinetics present a smaller but still significant discrepancy: + 28 mg/dm²/y when compared to + 2 mg/dm²/y. Weight variation is calculated with the weight measured after the 2nd cleaning with pure water, which is supposed as more reliable. Indeed, the weight is systematically lower, meaning metallic sodium was remaining on the surface layer of all specimens. Based on our recent feedback [16, 18, 20], this indicates that sodium remains on porosities created by the corrosion at the surface layer. Reaction of sodium with ethanol is incomplete or slow due to the formation of thin film of reaction products that controls the transfer of ethanol to sodium.

These 2 distinct behaviours are from then on referred to oxidation and dissolution for convenience.

III.A. Oxidation characterisation

This feature is observed for specimen exposed after the first exposure period up to the last period of test (periods 2+3+4+5, 3+4+5, 4+5 and 5). Their appearance is mostly metallic, with black patches for 3900h (periods 2+3+4+5), but evolves to complete black layer for the last 650h of the test (period 5). Fig. 1 shows an example of the typical oxide surface of samples corroded during 3900 h at 550°C, observed with the SEM. Triangular shaped crystals are observed on the surface; EDX analyses show that these ~1 µm-large crystallites are chromium, sodium and oxygen-rich. Based on previous and numerous observations that included XRD analyses [16, 18], these crystals correspond to sodium chromite. Below these crystallites, small grains rich in Mo and Fe of less than 100 nm in size are observed in between porosities.

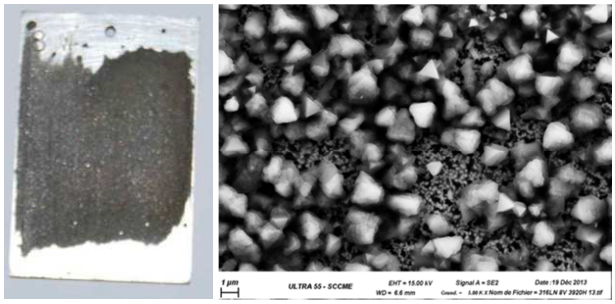

Fig. 1. Photo and SEM surface observation (secondary electrons) of the sample (20x30x1.5 mm) immersed during the last 3900 h (periods 2+3+4+5) of the test at 550 °C in liquid sodium with low oxygen content.

Both cross section observation of the oxide zone and GD-OES depth chemical elemental profiles (Fig. 2) confirms the typical morphology of $NaCrO_2$ formation: a quite uniform scale enriched in Na, Cr, and O is found at the interface. Its thickness is about 500 nm and seems not function of the exposure duration.

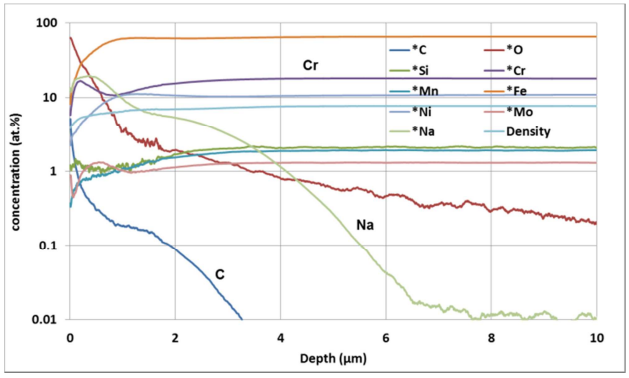

Fig. 2. GD-OES depth chemical profiles in log. scale of the oxide zone for the sample immersed during the last 3900 h (periods 2+3+4+5) of the test at 550 °C in liquid sodium with low oxygen content.

Then, a Cr depleted zone appears, large of about 1 µm, without indication of any preferential leaching of Ni compared to Fe. Its thickness is quite steady during the test. In between, a Mo enriched zone of about 0.1 to 0.2 µm in thickness is found. In addition, silicon appears slightly enriched in the Cr depleted zone, which might correspond to internal oxidation with formation of SiO_2 already observed [18, 21]. The sodium profile extends to 4 to 6 µm in depth corresponding to a sodium diffusion zone,

which represents the largest layer observed. This observation is not or little documented in the literature except in recent observations done within the same research group [16, 18-22], which is explained by the choice of the soft cleaning procedure and surface layer analysis by GDOES. Carbon shows as well diffusion-precipitation profile specific of carburation, which is more intense and larger than the one caused by EDM machining. This seems to be restricted to the Cr depleted zone.

The black patches are clearly identified as sodium chromite scale, whose thickness seems steady with the exposure time, but surface extension increase with the last period of test, even though the duration of the last period are shorter. To the contrary, the metallic zone of these samples shows features similar the surface of the specimen exposed since the beginning of the test that remained shiny.

III.B. Dissolution characterisation

The appearance of specimen immersed from the beginning of the test keeps metallic and shiny. It seems unaffected by the sodium with no apparent evolution with the exposure duration (periods 1 + n + m + …). Fig. 3 shows an example of the typical surface observed with the sample corroded during 4600 h at 550°C. However, the surface observed with SEM appears covered with grains of different size and nature to the notable exception of oxides.

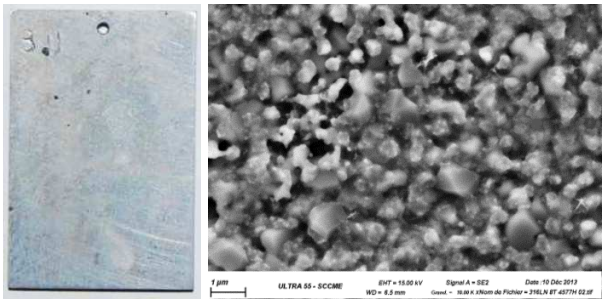

Fig. 3. Photo and SEM surface observation (secondary electrons) of the sample (20x30x1.5 mm) immersed from the beginning of the test for 4600 h at 550 °C in liquid sodium with low oxygen content.

A zone of high contrast in secondary electron, probably enriched in heavy element (Mo) is observed. The size ranges from 300 to 600 nm. The structure is similar to coral as it presents rounded shape with holes of about the same dimension (500 nm). The rest of the surface presents grains of matrix of 500 nm to 1 µm in size. These grains are separated with porosities that apparently increase in size with exposure duration. This zone may indicate a transitory state preceding the zone with high contrast.

These porosities contain traces of residual sodium, indicated by the SEM observation of the reaction products of sodium with air. Indeed, needles of sodium carbonates might be observed on some sample and sodium hydroxide is thought to blur SEM imaging. These products make a white veil on sample left in the open air for a few days. This veil reappears after cleaning as long as some sodium metal remains in these porosities. Lastly, faceted crystallites of about 1 µm in size are seen on surface as in Fig. 3, rich in Cr or Fe. Some others are rich in Cu (250 nm).

Both cross section observation of the dissolution zone and GD-OES depth chemical elemental profiles (Fig. 4) confirms the homogenous surface corrosion layer large of 3 to 4 µm after 4600h, which became almost steady after 1500h of sodium exposure. This surface layer is not related to any oxide except maybe for the first 200 nm, which is related to contamination after the sodium test.

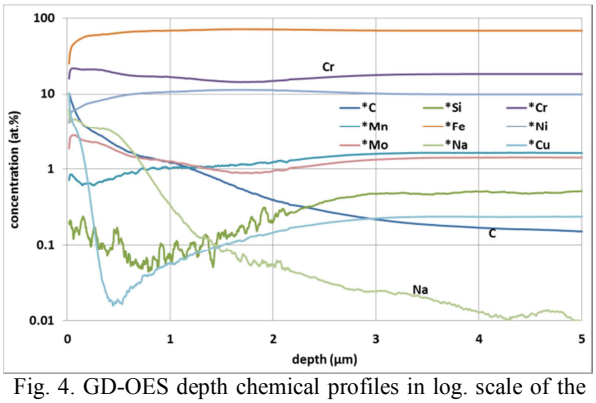

Fig. 4. GD-OES depth chemical profiles in log. scale of the dissolution zone for the sample immersed from the beginning of the test for 4600 h at 550 °C in liquid sodium with low oxygen content.

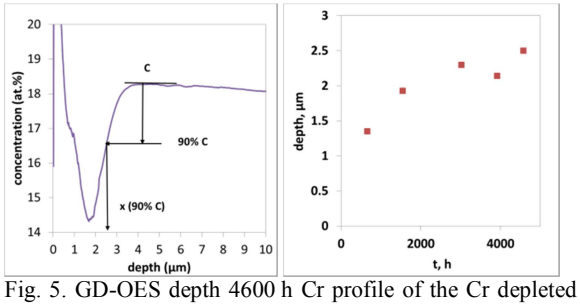

Fig. 5. GD-OES depth 4600 h Cr profile of the Cr depleted zone and method of estimation of the extent of Cr depleted zone (c : Cr concentration of the bulk, x : depth for 90% of c).

The carbon profile indicates a significant carburisation of the surface layer that includes both diffusion of carbon up to a 3 µm depth and carbides precipitation on the first 1 to 2 µm. Indeed, the change in slope for the carbon profile in the carbide zone corresponds with those for the Cr and Mo profiles. Cr and Mo both present enrichment in this zone together with C. In addition, carbon concentrations are as large as 0.5 to 2.5 atomic % when compared to the 0.12 at. % of the bulk. This zone is followed by a Cr and Mo depleted zone, whose extent is estimated by the depth corresponding to the moment when Cr content recovers

90% of its bulk value (Fig. 5). The depleted zone thickness becomes more or less steady after 3000h of sodium exposure with a value close to 2 – 2.5 µm.

No preferential leaching of Ni from the austenite matrix is observed, but this effect might be masked by the superposition of other effects. Indeed, a sodium diffusion zone is also present to a lesser extent than for oxidation: 5 µm at the most. The larger content in sodium on the first micrometer corresponds to porosities filled with sodium, which indicates the extent of these porosities in the surface layer, which seems to increase in size with sodium exposure duration.

Cu profile presents enrichment on the first 200 nm that corresponds to the Cu crystallites observed by SEM (mean size of about 200 nm). The source of copper comes from the 2-3 µm Cu depletion of the steel indicated by the same GD-OES profile, according to a dissolution mechanism followed by precipitation that might be delayed to the temperature decrease step for specimen extraction. Indeed, Cu solubility is assessed to 55 ppm in weight [2], and is analyzed on all samples (ethanol cleaning solution), indicating a mechanisms of mass transfer that occurred in between specimen through the liquid metal.

Features of the so called dissolution appeared as the superposition of carburization and dissolution. Although the dissolution mechanism's is not clearly evidenced, it appears related to the formation of cavities and dissolution of Fe and Ni (as well as Cu, which stands here for a marker for this mechanism) from the surface layer together with the formation of Mo rich nodules at the interface. Chemical analyses of the ethanol used to clean each independent specimen do not show any saturation effect of iron with increasing exposure duration, as the concentration continue to increase with exposure time, but present some effect of mass transfer and deposition between samples. As the surface layer presents carbide precipitation as well as sodium penetration, it is difficult to separate each effect independently. The weight variation is then the result of mass balance of each effect: loss of Fe, Ni and Cu by dissolution, gain of carbon and sodium by transfer from the liquid metal as well as mass transfer and precipitation as Cu or Fe crystallites at the interface. It cannot represent, as such, any dissolution kinetics. Further characterization was required.

III.C. Dissolution by TEM

The TEM characterization of the thin slice extracted by FIB technique from the 4600 h specimen (period 1+2+3+4+5) revealed the presence of various inclusions in the surface layer and crystallites precipitated on the surface (Fig. 6):

1- 90% Fe-rich grains of 400-800 nm in size in the surface layer, most probably ferrite;
2- Mo-rich grains of 200 nm in size at the interface, which may be carbide or Chi intermetallic phase;
3- Porosities of 500 nm in size, which may be grains ripped off during sodium test or sample preparation.
4- Fines inclusions of 10-50 nm in size in the Cr depleted zone, rich in Si and O (ratio ½); which corresponds to internal oxidation with SiO_2 formation;
5- Cr-rich spherical inclusions of 100 nm in size, which are intra-granular Chromium rich carbide and are noticeably absent from ferrite grains;
6- Cr-rich crystallites on the surface, which are Chromium carbide as confirmed by EELS techniques.

A chromium diffusion profile is measured below the chromium carbide precipitated at the surface by the EDX technique. The depth is about 1 µm, which agrees with the Cr depleted zone measured by the GD-OES. However, the profile is disturbed by Cr-rich carbide precipitated within the matrix, making it difficult to derive to a clear conclusion, except that the chromium content in the alloy of the surface layer is lower than in the alloy bulk.

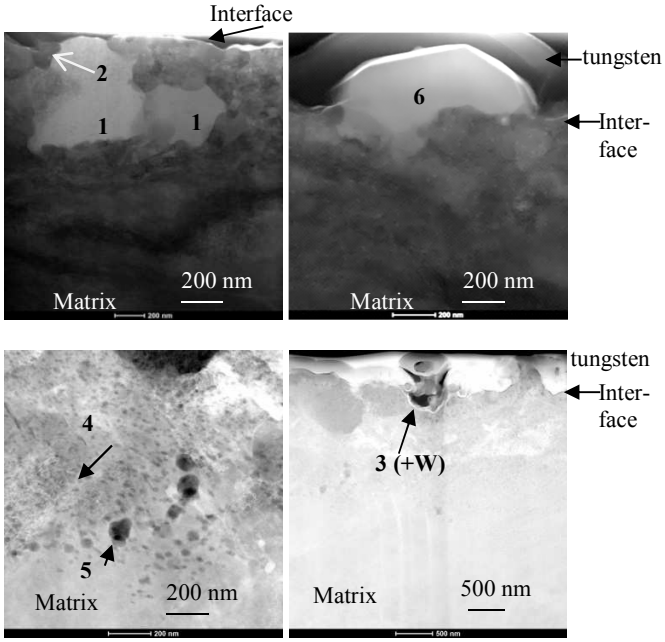

Fig. 6. Scanning transmission electron microscopy bright field imaging (top) and high angle annular dark field (Bottom) of surface layer of thin slice extracted by FIB from the surface of the sample immersed for 4600 h at 550 °C in liquid sodium with low oxygen content.

All previous observations are then confirmed and detailed: carbide precipitation on the surface (Cr_xC) as well as intra-granular carbide precipitation together with the formation a Cr-depleted zone of about 1 µm thick, where Ni seems to keep steady. The grains of ferrite present at the interface are either due to EDM machining artefact or due to the dissolution mechanism. This requires further examination before to conclude that this ferrite grains represent the first signs of the ferrite scale formation that

are formed by preferential dissolution of Ni in Cr depleted matrix.

In addition, internal oxidation markers are characterized, which must be further understood. Does it indicate an oxidation transient by formation of $NaCrO_2$, as it was already observed to go along with internal oxidation? This oxidation step should then have been followed by chromite scale reduction, proving the complexity of the various mechanisms at play in that kind of system depending on the fine variation of the chemistry of the liquid metal system.

III.D. Thermodynamic analysis

Both oxidation and carburisation result in the formation of Cr depleted zone. In order to understand how 2 separate mechanism of corrosion can happen at the same time during the sodium test, the source of contamination in carbon and oxygen must first be discussed before to go for thermodynamic analysis.

During this corrosion test performed in static conditions, the liquid metal chemistry may have derived by 2 factors. First, a gradual contamination in oxygen occurs at each extraction of specimen, as it requires opening the setup. The liquid sodium at 120°C gets into contact with the argon, which cannot be sufficiently purified as regards sodium. This contamination is arbitrarily assessed to a few ppm corresponding to the saturation at 120°C, but no justification could be given that higher contamination by supersaturation was prevented. Higher oxygen content by a few ppm is then expected at the beginning of each exposure period. Unfortunately, no means of oxygen monitoring exists for the moment for such low level of dissolved oxygen despite the developments pursued within the laboratory for vacuum distillation implementation and oxygen sensor development by mean of innovative ceramic [23]. Secondly, carbon is an unavoidable impurity in sodium [24], especially for newly prepared sodium where any buffer effects with structures are prevented. It presents a large carbon activity with dissolved species able to carburize the alloys by carbon transfer (Na_2C_2). It is thought that carbon might decrease with the exposure time that would explain why the competition in between the 2 mechanisms goes in favor of oxidation when compared to carburization at the end of the test.

As a conclusion, the initial content in oxygen that was low thanks to the initial purification gradually increased with the exposure time by a few ppm, while the initial carbon content that was initially high may have gradually decreased because of its consumption for carburizing the specimens.

The threshold oxygen content for the precipitation of sodium chromite can be assessed by thermodynamic analysis. Fig. 7 represents the oxygen potentials plotted on an Ellingham kind diagram as a function of temperature with either different oxygen activities in liquid sodium or different chromium activities at the reactive interface as parameters [21]. The red dotted line represents the constant concentration line for 10 ppm in weight that represents roughly the upper threshold for reactor operations.

For steady temperature system, the critical oxygen content for the formation of $NaCrO_2$ depends on the chromium activity: the lower the higher the oxygen required. Fig. 7 plotted the equilibrium line for various Cr activities: 1 for pure chromium metal and 0.32 for 316LN [25]. Experimental observations on 316L are also plotted and fitted [26], corresponding most probably to a chromium activity lower than the alloy bulk activity because of the Cr depletion of the surface layer in a way very similar to our observations.

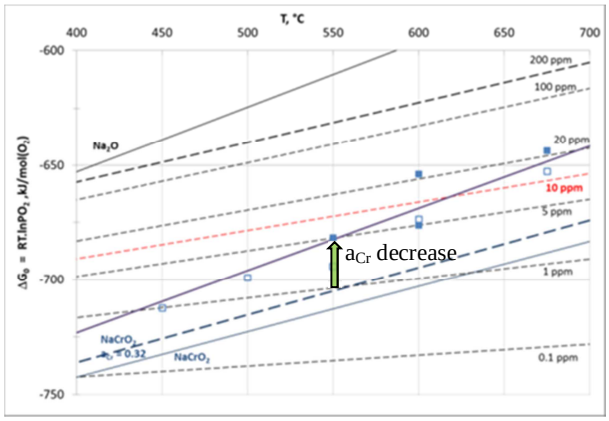

Fig. 7. Oxygen potentials in the Cr-O-Na system as function of temperature for sodium oxide and chromite oxide formation (Free energies of formation for Na_2O and $NaCrO_2$ from Hsc. 5.11 software, Thorley oxygen solubility relation, experimental observations of sodium chromite on 316L plotted as full square with mean squared fitting [26])

In others words, the oxidation depletes the surface layer in chromium, lowering the Cr activity and increasing the oxygen concentration required for further oxidation into $NaCrO_2$. The oxidation zone in the diagram is then decreased in surface to the profit of the dissolution zone. Supposing that a small contamination in oxygen gives an oxygen concentration lower than the new oxidation threshold, then the steel specimen will not oxidize as the thermodynamic conditions are not fulfilled. If the specimen encountered first carburization with the formation of a similar Cr depleted surface layer, then these specimens will also not oxidize when compared to newly immersed specimen. In addition, if the total amount of oxygen of one contamination reacts with a comparatively smaller size when compared to the initial conditions where surface exposed to sodium were larger, then, the oxidation gets more significant. In other words, all of the available oxygen reacts with smaller surface yielding thicker oxide scale than expected with larger surface reaction.

V. CONCLUSIONS

In the end, even though the oxygen variation kept within a tiny range to prevent oxidation of Cr depleted surface layer, it was nonetheless enough to promote oxidation of newly immersed sample, giving the apparent opposed corrosion behavior of identical sample exposed to the same conditions. Oxygen level of the test may be assessed to lower than 5 ppm to prevent oxidation according to the thermodynamic data (Fig. 7). Issues are still pending and require further studies, such as the kinetics of the various corrosion steps involved (oxidation, reduction of the oxide scale, dissolution, carburization, mass transfer and precipitation, etc.).

Finally, the dissolution mechanisms occurred during the test but not in a separate way. It was either combined with oxidation or carburization, or with both of them. The accurate control of the liquid sodium chemistry proved complex and sensitive to little and unexpected variations. Sodium - steel systems appeared to obey to the thermodynamics to the condition to consider the surface layer of the steel in the system, which reaffirm the need for accurate data.

In an actual non isothermal circuit of a reactor, all these effects happen in the same way and are at the origin of the chemical buffering effects supposed or observed in such leak tight liquid metal systems. Tight application of purification procedures to limit to the minimum the total amount of oxygen in the system before high temperature operation is clearly the best corrosion control policy. Carbon cannot be purified specifically. Its activity will be buffered to an intermediate level when the liquid metal equilibrates with the structure. Carburization will enhance the Cr depletion of the surface layer in a similar way that oxidation. This means that new surface of component such as primary pump, intermediate heat exchangers, or fuel cladding pins will be more prone to oxidation during normal or off-normal chemical transients, such as restart after refueling, or contamination by air ingress, whereas all other structure may well stay in their so-called ‘dissolution’ domain. As a consequence, all of the available oxygen will oxidize this small fraction of the total surface and not be distributed on all structures, which would have constituted a more favorable case. Small contamination of a few ppm might then be enough to concentrate the oxide scale formation on little surfaces with potentially adverse consequences. Such behaviors are to be investigated.

REFERENCES

1. Cabet, C., D. F., M. Sauzay, Y. Cui, L. Forest, J.L. Courouau, S. Dubiez-Le Goff, T. Marlaud, and M. Blat-Yrieix, Some recent results on stainless steel 316L(N) for a 60 years design life as ASTRID structural material in ICAPP 2014, Charlotte, USA.
2. Borgstedt, H.U. and C.K. Mathews, Applied chemistry of the alkali metals, 1987, New-York, Plenum Press.
3. Furukawa, T., S. Kato, and E. Yoshida, Compatibility of FBR materials with sodium, Journal of Nuclear Materials, 2009, 392(2), p. 249.
4. Balbaud-Célérier, F., P. Arnoux, C. Cabet, J.-L. Courouau, and L. Martinelli, Corrosion of structural materials for Generation IV systems, ICAPP 2009. Tokyo, Japan.
5. Courouau, J.-L., V. Lorentz, and F. Balbaud, Sodium corrosion studies in support of SFR: State of the art, 3rd International Topical Seminar JAEA/CEA on Coolant and Innovative Reactor Technologies (Gédépéon), 2009, Aix-en-Provence, France.
6. Courouau, J.-L., F. Balbaud-Célérier, V. Lorentz, and T. Dufrenoy, Corrosion by liquid sodium of materials for sodium fast reactors: the CORRONa testing device, ICAPP 2011, Nice, France.
7. Balbaud-Célérier, F., J.-L. Courouau, C. Desgranges, L. Martinelli, and F. Rouillard, Corrosion of the Fe-9Cr steels in sodium fast reactors environments, ICAPP 2011, Nice, France (SFEN-RGN 2011 n°5 sept.-Oct. pp87-97).
8. Weeks, J.R. and H.S. Isaacs, A general model for the corrosion of steels in high velocity sodium, in Chemical aspects of corrosion and mass transfer in liquid sodium. 1973. October 19--20, 1971, Detroit, Michigan, USA.
9. Kolster, B.H., Mechanism of Fe and Cr transport by liquid sodium in non-isothermal loop systems, Journal of Nuclear Materials, 1975, 55(2), p. 155.
10. Brissonneau, L., New considerations on the kinetics of mass transfer in sodium fast reactors: an attempt to consider irradiation effects and low temperature corrosion, Journal of Nuclear Materials, 2012, 423(1-3): pp. 67-78.
11. Thorley, A.W. and J.A. Bardsley, Structural changes in materials exposed to liquid sodium, Journal of the Royal Microscopical Society, 1968, 88(4): pp. 431-447.
12. Baque, P., A. Lapon, E. Sermet, and L. Champeix, Contribution à l'étude de la corrosion de l'acier austénitique bas carbone (afnor Z3 CN 18-10) par le sodium liquide à 700°C, Journal of Nuclear Materials, 1974, 54(2): pp. 241-244.
13. Ganesan, V., V. Ganesan, and H.U. Borgstedt, Analysis of CREVONA sodium loop material, Journal of Nuclear Materials, 2003, 312(2-3): p. 174.
14. Cavell, I.W. and M.G. Nicholas, Some observations concerned with the formation of sodium chromite on AISI 316 exposed to oxygenated sodium, Journal of Nuclear Materials, 1980, 95(1-2): pp. 129-144.
15. Borgstedt, H.U., Compatibility of steel No. 1.4970 with liquid sodium at high temperatures, Journal of Nuclear Materials, 2003, 317(2-3): p. 160.
16. Rivollier, M., J.L. Courouau, M.-L. Giorgi, F. Jomard, V. Lorentz, and M. Tabarant, Oxidation of 316LN

stainless steel in liquid sodium at 650°C, EUROCORR 2014, Pisa, Italy (EFC).
17. Shaiu, B.J., P.C.S. Wu, and P. Chiotti, Thermodynamic properties of the double oxides of Na_2O with the oxides of Cr, Ni and Fe, Journal of Nuclear Materials, 1977, 67(1–2): pp. 13-23.
18. Courouau, J.-L., V. Lorentz, M. Tabarant, S. Bosonnet, and F. Balbaud-Célérier, Corrosion by oxidation and carburization in liquid sodium at 550°C of austenitic steels for sodium fast reactors, Fast Reactors 2013 (FR13), 4-7 March, Paris, France.
19. Rivollier, M., J.L. Courouau, M.-L. Giorgi, F. Jomard, M. Tabarant, C. Blanc, and S. Vaubaillon, Study of the Oxidation Mechanisms of 316LN Steel in Liquid sodium, ICAPP 2015 (paper 15407), Nice, France.
20. Hémery, S., T. Auger, J.L. Courouau, and F. Balbaud-Célérier, Liquid metal embrittlement of an austenitic stainless steel in liquid sodium, Corrosion Science, 2014, 83(0): pp. 1-5.
21. Courouau, J.-L., M. Tabarant, R. F., T. S., F. Balbaud-Célérier, V. Lorentz, and C. Cabet, Corrosion by oxidation and carburization in liquid sodium at 550°C of Fe-9Cr steels for sodium fast reactors (poster), International Workshop on Structural Materials for Innovative Nuclear Systems (SMINS3), 2013. 7-10 Oct.2013, Idaho Falls, USA.
22. Hémery, S., T. Auger, J.L. Courouau, and F. Balbaud-Célérier, Effect of oxygen on liquid sodium embrittlement of T91 martensitic steel, Corrosion Science, 2013, 76(0): pp. 441-452.
23. Fouletier, J. and V. Ghetta, Potentiometric Sensors for High Temperature Liquids, in Materials Issues for Generation IV Systems, NATO Science for Peace and Security Series B: Physics and Biophysics 2008. pp. 445-459.
24. Gnanasekaran, T. and C.K. Mathews, Threshold oxygen levels in sodium necessary for the formation of $NaCrO_2$ in sodium-steel systems, Journal of Nuclear Materials, 1986, 140(3): p. 202.
25. Pillai, S.R., H.S. Khatak, and J.B. Gnanamoorthy, Formation of $NaCrO_2$ in sodium systems of fast reactors and its consequence on the carbon potential, Journal of Nuclear Materials, 1995, 224(1): p. 17.
26. Nicholas, M.G. and I.W. Cavell, The formation of sodium chromite on AISI 316 and other sodium containing alloys, Second international conference on liquid metal technology in energy production, 1980, Richland, Washington (ANS conf-800401 p2, UC-79A).